Microscopy, 2022, **71(2)**, 98–103
DOI: https://doi.org/10.1093/jmicro/dfab055
Advance Access Publication Date: 11 January 2022
Article

MICROSCOPY

Study of high–low KPFM on a pn-patterned Si surface

Ryo Izumi, Yan Jun Li*, Yoshitaka Naitoh and Yasuhiro Sugawara

Department of Applied Physics, Graduate School of Engineering, Osaka University, 2-1 Yamadaoka, Suita, Osaka 565-0871, Japan
*To whom correspondence should be addressed. E-mail: liyanjun@ap.eng.osaka-u.ac.jp

Abstract

Comparative measurements between frequency modulation Kelvin probe force microscopy (FM-KPFM) using low frequency bias voltage and heterodyne FM-KPFM using high frequency bias voltage were performed on the surface potential measurement. A silicon substrate patterned with p- and n-type impurities was used as a quantitative sample. The multi-pass scanning method in the measurements of FM-KPFM and heterodyne FM-KPFM was used to eliminate the effect of the tip–sample distance dependence. The measured surface potentials become lower in the order of the p-type region, n-type region and n^+-type region by both FM-KPFM and heterodyne FM-KPFM, which are in good agreement with the order of the work functions of the pn-patterned Si sample. We observed the difference in the surface potentials due to the surface band bending measured by FM-KPFM and heterodyne FM-KPFM. The difference is due to the fact that the charge transfer between the surface and bulk levels may or may not respond to AC bias voltage.

Key words: heterodyne, FM-KPFM, CPD, surface potential, Si, band bending

Introduction

The surface and interface states of semiconductors have a considerable effect on the reliability of semiconductor devices such as metal-oxide-semiconductor field-effect transistors (MOS-FETs) [1–4]. Since the surface states of semiconductors are related to their surface potentials, information on the surface potentials of semiconductors is important because it provides important insights into the electrical properties of the surface. To understand and control the surface states of semiconductor devices, it is important to measure the surface states of semiconductors, especially the surface potential, with high spatial resolution.

Kelvin probe force microscopy (KPFM) is a technique for measuring the surface potential of a sample with high spatial resolution [5–10]. KPFM is based on atomic force microscopy (AFM) [11–13]. The underlying principle of KPFM is that the contact potential difference (CPD) between the tip and the sample surface is detected from the change in the resonance frequency or amplitude of the cantilever by applying an AC bias voltage [7,14]. The AC bias voltage modulates the electrostatic interaction force between the tip and the sample. A DC bias voltage is used to nullify the average electrical force related to the CPD. The results of surface potential measurements of metals [15], semiconductors [8,9,16–20] and insulators [21,22] by KPFM have been reported.

It has been reported that the results of KPFM reflect the condition of surface states. According to Ref. [14], increasing the concentration of impurities in a semiconductor causes band bending near the semiconductor surface; as a result, the CPD values deviates from those expected from the bulk states. Therefore, the CPD values measured by KPFM are affected by both the surface and bulk states. Separating bulk and surface information is important for understanding the electronic states of semiconductor surfaces and bulks.

To distinguish the information of the surface state from that of the bulk state in KPFM, it is very effective to use the frequency dependence of the AC bias voltage. This idea can be explained as follows. When an AC bias voltage is applied between the probe and the surface in KPFM, the Fermi level of the tip changes up and down with respect to the surface and bulk Fermi levels. There is a limit of the response rate of electron emission from the surface state to the bulk state [1,23]. As a result, the electron transfer between the surface state and the bulk state is strongly influenced by the frequency of AC bias voltage. That is, at frequencies lower than the cutoff frequency (fc) (<100 kHz), which is determined by the rate of charge capture and emission at the surface state, charge transfer occurs between the surface and bulk states, resulting in an up and down band bending [1,23]. On the other hand, at frequencies higher than fc (> several 100 kHz), charge transfer between the surface state and bulk state is less likely to occur, resulting in a slower response of the surface state and less change in band bending.

In KPFM, three major measurement modes have been used [7]: frequency modulation KPFM (FM-KPFM), amplitude modulation KPFM (AM-KPFM) and heterodyne AM-KPFM. In FM-KPFM, an AC bias voltage at the frequency (< 1 kHz) within the bandwidth of the phase-locked loop (PLL) is applied, and the modulation component of the frequency shift of the cantilever is used to measure the CPD values. In AM-KPFM, an AC bias voltage near/at the first (or second) resonance frequency of the cantilever is applied, and the cantilever deflection at the first (or second) resonance frequency is used to measure the CPD values. In heterodyne AM-KPFM, an AC bias voltage at the frequency of the difference between the first and second resonance frequencies is applied, and the cantilever deflection at the second (or first) resonance frequency is

Received 26 October 2021; Revised 30 November 2021; Editorial Decision 5 December 2021

used to measure the CPD values. Thus, FM-KPFM uses a low-frequency AC bias voltage, while AM-KPFM and heterodyne AM-KPFM use a high-frequency AC bias voltage. FM-KPFM and AM-KPFM (Heterodyne AM-KPFM) use different force detection modes, FM mode and AM mode, respectively, and it is difficult to switch between the two force detection modes, making it difficult to perform low and high frequency KPFM measurements at the same position on the sample surface.

Recently, we proposed a new KPFM, the heterodyne FM-KPFM, which uses the FM mode as the force detection mode [18]. This method is based on the heterodyne effect of cantilever vibration and electrostatic force and allows the use of high frequency AC bias without increasing the bandwidth of the cantilever deflection sensor, with only minor changes to the FM-KPFM configuration. By alternating between FM-KPFM and heterodyne FM-KPFM using low and high frequency AC bias voltages, respectively, we have demonstrated that we can separate the surface state information from the bulk state information of reduced TiO_2(110) samples [18]. Hereafter, we refer to this method as high–low KPFM (HL-KPFM). In the reduced TiO_2 sample, the effectiveness of HL-KPFM has not been fully discussed because the density of oxygen defects is unknown and the carrier concentration is also unknown; therefore, the use of a sample that can be discussed more quantitatively has been desired.

In this study, to demonstrate the effectiveness of HL-KPFM on the surface potential measurement, we performed comparative study between FM-KPFM measurement and heterodyne FM-KPFM measurement using a silicon substrate patterned with p- and n-type impurities as a quantitative sample. The measured surface potentials become lower in the order of the p-type region, n-type region and n^+-type region by both FM-KPFM and heterodyne FM-KPFM, which are in good agreement with the order of the work functions of the pn-patterned Si sample. We observed the difference in the surface potentials measured by FM-KPFM and heterodyne FM-KPFM, which is due to the surface band bending.

Theory

FM-KPFM

First, we explain the operation principle of FM-KPFM. When bias voltage V is applied between the tip and the sample, the electrostatic force between the tip and the sample can be expressed by considering the tip–sample system as capacitor and can be written as follows:

$$F_{\mathrm{ele}} = \frac{1}{2}\frac{\partial C}{\partial z}(V - V_{\mathrm{CPD}})^2 \tag{1}$$

where C, z and V_{CPD} are the capacitance, the distance and the CPD between the tip and the sample, respectively. Here, the electrostatic force is always attractive interaction because $\partial C/\partial z < 0$. (Denominated z-direction, electrostatic force perpendicular to the sample surface.) In FM-KPFM, $V = V_{\mathrm{DC}} + V_{\mathrm{AC}}\cos\omega_{\mathrm{m}}t$ is applied, where V_{DC} is the DC bias voltage, and V_{AC} and ω_{m} are the amplitude and the modulation frequency of the AC bias voltage, respectively. By expanding the equation, we can show that the electrostatic force contains the component of modulation frequency ω_{m} as follows:

$$F_{\mathrm{ele}}(\omega_{\mathrm{m}}) = \frac{\partial C}{\partial z}V_{\mathrm{AC}}(V_{\mathrm{DC}} - V_{\mathrm{CPD}}) \tag{2}$$

In frequency modulation atomic force microscopy (FM-AFM), the modulation component of the frequency shift $\triangle f\ (\omega_m)$ due to the electrostatic force $F_{\mathrm{ele}}\ (\omega_m)$ is expressed by the following equation:

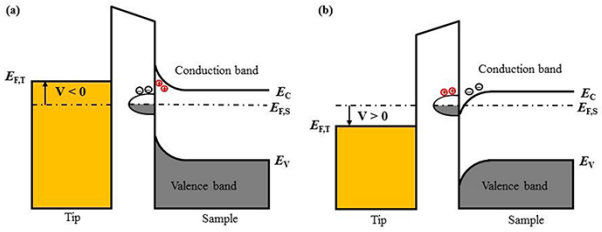

Fig. 1. Schematic diagrams of field-effect-induced (lower frequency of AC bias voltage) band bending on n-type semiconductor with surface states and carriers transition between the surface state and bulk state. (a) $V < 0$ and (b) $V > 0$. Here, the surface-state-induced band bending is included and it shows the equilibrium between n-type bulk and its surface. (For simplicity, the work functions of the tip and the semiconductor are assumed to be the same.)

$$\Delta f(\omega_{\mathrm{m}}) \simeq \frac{f_0}{k}\frac{\partial^2 C}{\partial z^2}V_{\mathrm{AC}}(V_{\mathrm{DC}} - V_{\mathrm{CPD}}) \tag{3}$$

where f_0 $(=\omega_0/2\pi)$ and k are the resonance frequency and the effective spring constant of the cantilever, respectively. In KPFM, the DC bias voltage is feedback-controlled so that the ω_{m} component of the frequency shift $\triangle f\ (\omega_{\mathrm{m}})$ becomes zero during scanning of the sample surface. The V_{CPD} can be measured by recording the DC bias voltage when $\triangle f\ (\omega_{\mathrm{m}})$ becomes zero by feedback control.

Note that in FM-KPFM, the modulation frequency ω_{m} is less than 2 kHz because the signal-to-noise ratio of the modulation component of the frequency shift $\triangle f\ (\omega_{\mathrm{m}})$ is degraded with increasing ω_{m} [24]. Here, we consider the carrier transfer between the accepter-like surface state (the dangling bond states) and bulk states, taking the n-type semiconductor as an example. In this case, electrons move so that the Fermi level of the surface level is equal to the bulk Fermi level, the surface level is negatively charged, the subsurface is positively charged, and the band bends upward at the surface, as shown in Fig. 1. When an AC bias voltage is applied between the tip and the surface, the Fermi level of the tip moves up or down with respect to the surface-state level. At frequencies ω_{m} lower than the cutoff frequency (f_{c}) (<100 kHz), which is determined by the rate of charge capture and emission at surface states [1,23], the charge transfer between the surface states and bulk states easily occurs, and hence the band bending changes upwardly and downwardly. As a result, the V_{CPD} measured by FM-KPFM using low frequency AC bias voltage contains information on both the bulk Fermi level and the surface band bending.

Heterodyne FM-KPFM

Next, we explain the theory of heterodyne FM-KPFM. The general setup of which is shown in Fig. 2. We consider the case where the cantilever is vibrating with amplitude A and angular frequency ω_0. We can express the position of the tip of the cantilever as $z = z_0 + A\cos\omega_0 t$, where z_0 is the mean distance between the tip and the surface. The capacitance between the tip and the sample depends on the distance between the tip and the sample. As a result, the capacitance voltage gradient $\partial C/\partial z$ can be expanded as

$$\frac{\partial C(z)}{\partial z} \simeq \frac{\partial C(z_0)}{\partial z} + \frac{\partial^2 C(z_0)}{\partial z^2}A\cos\omega_0 t \tag{4}$$

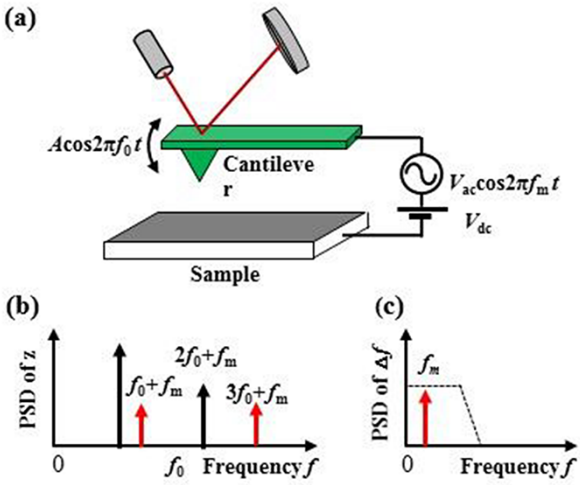

Fig. 2. Schematic view of electrostatic interaction between tip and sample and PSD as function of frequency in heterodyne FM-KPFM. (a) Electrostatic interaction between tip and sample by applying V_{DC} and V_{AC} with frequency $2f_0 + f_m$. (b) PSD of deflection z of frequency. (c) PSD of frequency shift Δf as a function of frequency.

By substituting Eq. (4) into Eq. (1), we can write the electrostatic force as

$$F_{ele} \simeq \frac{1}{2}\frac{\partial C(z_0)}{\partial z}(V - V_{CPD})^2 + \frac{1}{2}\frac{\partial^2 C(z_0)}{\partial z^2}(V - V_{CPD})^2 A\cos\omega_0 t \quad (5)$$

In heterodyne FM-KPFM, the following bias voltage is applied between the tip and the sample:

$$V = V_{DC} + V_{AC}\cos(2\omega_0 + \omega_m)t \quad (6)$$

By expanding the second term of Eq. (5), one can see that the $\omega_0 + \omega_m$ component of the electrostatic force is included:

$$F_{ele}(\omega_0 + \omega_m) = \frac{1}{2}\frac{\partial^2 C(z_0)}{\partial z^2} V_{AC}(V_{DC} - V_{CPD})A \quad (7)$$

Now, we consider the frequency shift formula:

$$\Delta f = -\frac{f_0^2}{kA}\int_0^T F_{ele}(t)\cos\omega_0 t dt \quad (8)$$

As a result of the electrostatic force $F_{ele}(\omega_0 + \omega_m)$, it can be seen that frequency shift Δf (ω_m) measured in FM mode is expressed as

$$\Delta f(\omega_m) = \frac{f_0}{2k}\frac{\partial^2 C(z_0)}{\partial z^2} V_{AC}(V_{DC} - V_{CPD}) \quad (9)$$

In heterodyne FM-KPFM, as well as FM-KPFM, the V_{CPD} can be measured by recording V_{DC} when Δf (ω_m) becomes zero by feedback control. In heterodyne FM-KPFM, the AC bias voltage with high frequency is applicable. When frequency $2f_0 + f_m$ is higher than fc (>several 100 kHz), the charge transfer between the surface states and the bulk states does not occur, and hence the band bending does not change owing to the slow response of the surface state. As a result, the V_{CPD} measured by heterodyne FM-KPFM using high frequency AC bias voltage mainly contains information on the bulk Fermi level.

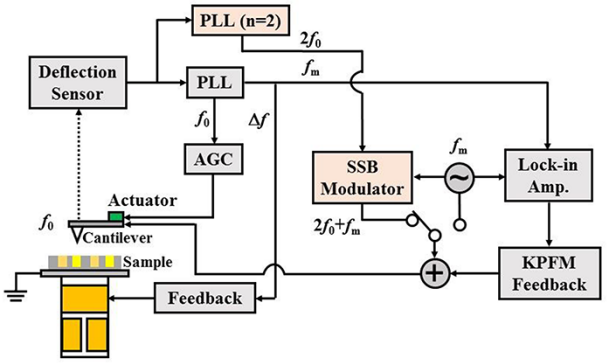

Fig. 3. Block diagram of FM-KPFM and heterodyne FM-KPFM setup. Here, FM-KPFM is shown in grey and heterodyne FM-KPFM in pink. Note that an AC signal of $\cos 2\omega_0 t$ is generated by PLL ($n = 2$, the second harmonic mode). An AC bias signal of $\cos(2\omega_0 + \omega_m)t$ is generated by the SSB modulator. For more details, see Ref. [19].

Experimental details

Figure 3 shows the block diagram of FM-KPFM and heterodyne FM-KPFM combined with FM-AFM. Here, FM method is used to detect the force interaction between the tip and the sample. The frequency shift of cantilever Δf is detected by using PLL circuit (Zurich Instruments: HF2PLL) by controlling oscillating amplitude A of the cantilever to be constant. Topographic images of the sample are obtained by controlling the distance between the tip and the sample so that frequency shift Δf is constant. In FM-KPFM, an AC bias voltage $\cos\omega_m t$ is generated by the local oscillator. In heterodyne FM-KPFM, an AC signal $\cos 2\omega_0 t$ is generated by PLL under the second harmonic mode ($n = 2$) synchronized with the cantilever oscillation. An AC bias voltage of $\cos(2\omega_0 + \omega_m)t$ is generated by mixing the signal of $\cos 2\omega_0 t$ with that of $\cos\omega_m t$ using a single sideband (SSB) modulator. In both FM-KPFM and heterodyne FM-KPFM, the ω_m component of frequency shift Δf_m is measured with a lock-in amplifier and used to regulate the DC bias voltage V_{dc}. KPFM images are obtained by regulating V_{dc} to nullify Δf_m. The experiment was performed in a vacuum environment at room temperature using a commercially available atomic force microscope (JEOL: JSPM-4210).

As a sample, a silicon substrate regularly doped with p- and n-type impurities was used. Figure 4 shows the pn-patterned Si substrate. The dopant pattern on the sample surface was formed by ion implantation. The p-type region was formed by implanting BF_2 ions with a dose of $7.0 \times 10^{12}/cm^2$ at 70 keV into a phosphorus-doped n-type Si substrate with a dopant concentration of $1 \times 10^{15}/cm^3$. The n+-type region was formed by implanting As ions with a dose of $3.0 \times 10^{12}/cm^2$ at 120 keV into the Si substrate. Impurity concentrations in the n, p and n^+ regions are $n = 1 \times 10^{15}/cm^3$, $p = 2 \times 10^{16}/cm^3$ and $n^+ = 5 \times 10^{19}/cm^3$, respectively. The density of doping is same as [19], while the pattern is different.

As a force sensor, a gold-coated cantilever (Mikromasch: HQ: NSC15/CR-AU) was used. The resonance frequency, spring constant and Q value of the cantilever are $f_{res} = 257.57$ kHz, $k = 40$ N/m and $Q = 10\,709$, respectively.

To investigate the frequency dependence of the AC bias voltage of V_{CPD}, the tip–sample distance in both FM-KPFM and heterodyne FM-KPFM measurements must be equal, because the V_{CPD} also depends on the tip–sample distance

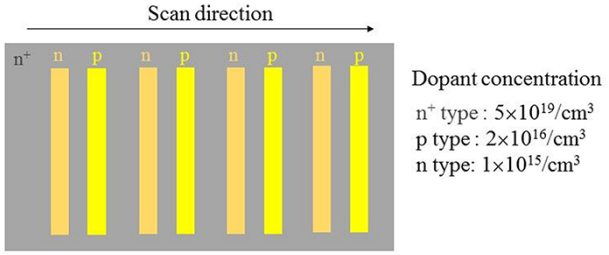

Fig. 4. Model of the pn-patterned Si substrate. The scan direction of surface imaging was performed as shown by arrow.

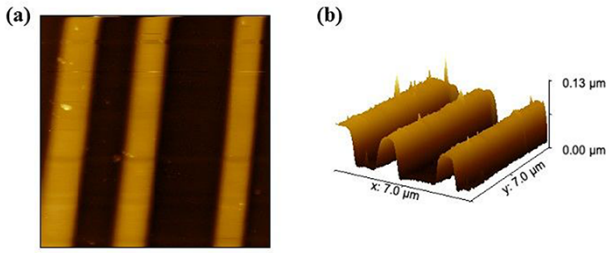

Fig. 5. (a) Wide range topographic image on the pn-patterned Si surface by FM-AFM experiment and (b) 3D image. Scan size: 7 μm × 7 μm.

[5–7]. Therefore, we used the multi-pass scanning method in the measurements of FM-KPFM/AFM and heterodyne FM-KPFM/AFM to eliminate the effect of the tip–sample distance dependence. In the first lateral scan, AFM measurement was performed while FM-KPFM measurement was performed. In the second lateral scan, heterodyne FM-KPFM measurement was performed with the trajectory of the first AFM measurement. The frequencies of the AC bias voltage applied between the tip and the sample were $f_m = 100$ Hz for FM-KPFM and $2f_0 + f_m = 515.232$ kHz for heterodyne FM-KPFM, respectively. The amplitude of the AC bias voltage was set to $V_{AC} = 0.5$ V to allow comparison of V_{CPD} measurements with a high signal-to-noise ratio for both FM-KPFM and heterodyne FM- KPFM. The oscillation amplitude of the cantilever was $A = 15$ nm.

Results and discussion

Figure 5a and b shows the topographic image of pn-patterned Si substrate and its 3D image, respectively. By comparing the topographic image in Fig. 5 and the model in Fig. 4, we can see that the surface is higher in the p- and n-type regions than in the n^+-type region.

Figure 6a and d shows the topographic image measured on a pn-patterned Si substrate and the cross-sectional profile along the red line in Fig. 6a. Figure 6b and c shows CPD images simultaneously obtained by FM-KPFM and heterodyne FM-KPFM, respectively, and Fig. 6e shows the cross-sectional profiles along the blue and green lines in Fig. 6b and c. From the topographic image in Fig. 6a and the line profile in Fig. 6d, we can see that the heights of the p- and n-type regions are almost equal. In contrast, in Fig. 6b, the CPD image by FM-KPFM, the p-type region is brightest, the n-type region is slightly darker and the n^+-type region is darkest. Similarly, in Fig. 6c, the CPD image by heterodyne FM-KPFM, the p-type region is brightest, the n-type region is

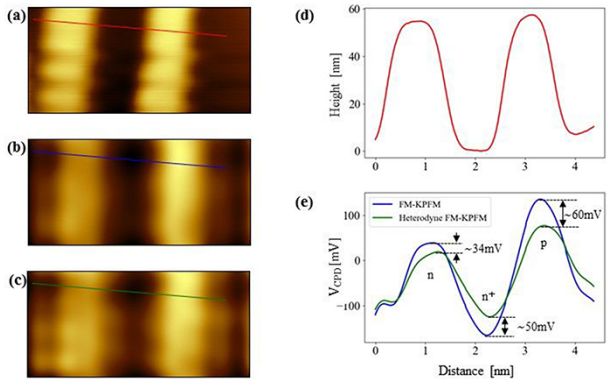

Fig. 6. AFM and surface potential images of pn-patterned Si surface using HL-KPFM method. (a) Topographic and (b) V_{CPD} images obtained by FM-KPFM with modulation frequency $f_m = 100$ Hz. (c) V_{CPD} image obtained by heterodyne FM-KPFM with $2f_0 + f_m \cong 515.2$ kHz. The scan size is 5 μm × 2.36 μm. (d) Line profile along red line in (a). (e) Line profiles along blue line in (b) and along green line in (c). Note that the CPD values are different in the n- and p-type regions. The CPD differences between the n, n^+ and p regions are due to the Fermi level differences between dopant regions. (n^+-type region, acceptor-like; n- and p-type regions, donor-like).

slightly darker and the n^+-type region is darkest. From the line profiles in Fig. 6e, we can see that the V_{CPD} values measured by both FM-KPFM and heterodyne FM-KPFM become lower in the order of the p-type region, n-type region and n^+-type region. These experimental results are in good agreement with the order of the work functions of pn-patterned Si samples [19].

Interestingly, in Fig. 6e, the line profile of the V_{CPD} values obtained by FM-KPFM is significantly different from those obtained by heterodyne FM-KPFM. In the p- and n-type regions, the V_{CPD} values obtained by heterodyne FM-KPFM become lower than those obtained by FM-KPFM, while in the n+-type region, the V_{CPD} values obtained by heterodyne FM-KPFM become higher than those obtained by FM-KPFM. This is the first result that the V_{CPD} values obtained by KPFM measurement strongly depend on the frequency of the AC bias voltage.

Next, we quantitatively investigate the V_{CPD} values in the n-, n^+- and p-type regions. The V_{CPD} values obtained by FM-KPFM are estimated to be +43 mV, −170 mV and +140 mV near the centers of the n-, n^+- and p-type regions, respectively (Fig. 7a). The V_{CPD} values obtained by heterodyne FM-KPFM are estimated to be +9 mV, −120 mV and +80 mV near the centers of the n-, n^+- and p-type regions, respectively (Fig. 7b). Therefore, the V_{CPD} values obtained by heterodyne FM-KPFM varied by −34 mV, +50 mV and −60 mV near the centers of the n-, n^+- and p-type regions, respectively, compared to those obtained by FM-KPFM. Here, + and − indicate that the band bending occur upwardly and downwardly at the surface, respectively. These experimental results mean that the band bending occur downwardly, upwardly and downwardly, the n-, n^+- and p-type regions, respectively.

If the surface state created by the broken atomic bonds exists near the center of the band gap, then in the case of an n-type semiconductor, electron transfer occurs from the bulk state to the surface state and the band bending is upward, while in the case of a p-type semiconductor, electron transfer

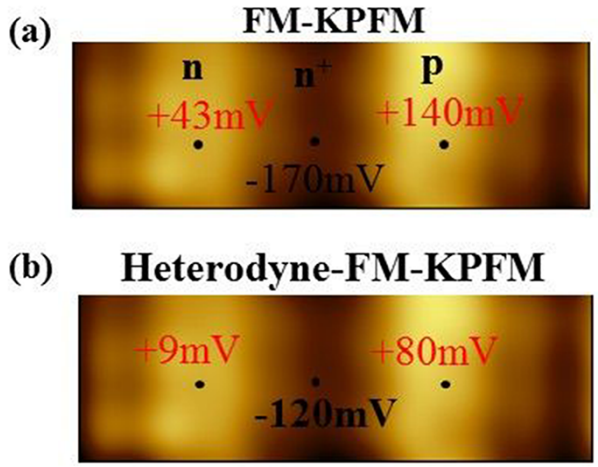

Fig. 7. Surface potential image on a pn-patterned Si semiconductor with acceptor-like (n^+-type region) and donor-like (n- and p-type regions) surface states. (a) V_{CPD} images obtained by FM-KPFM and (b) heterodyne FM-KPFM. Scan size: 5 μm × 1.70 μm. +43 mV on n-type region determined by FM-KPFM (+9 mV: by heterodyne FM-KPFM), −170 mV on n^+-type region determined by FM-KPFM (−120 mV: by heterodyne FM-KPFM) and +140 mV on p-type region determined by FM-KPFM (+80 mV: by heterodyne FM-KPFM).

occurs from the surface level to the bulk level and the band bending is downward. The experimental result in Fig. 7 that the band bending is upward in the n^+-type region and downward in the p-type region is consistent with the above model of electron transfer, but the experimental result that the band bending is downward in the n-type region is not consistent with the above model of electron transfer.

There are two possible causes for the downward band bending in the n-type region: first, many defects may have formed on the sample surface due to ion implantation, and these defects may have formed donor-like surface states; second, a natural oxide film may have formed on the surface, and donor-like interface states may have formed between the natural oxide film and the substrate. In either case, unlike the ideal acceptor-like surface state, a donor-like surface state was formed, and electron transfer from the donor-like surface state to the bulk state may have occurred, causing the band to bend downward.

Concluding remarks

We performed comparative measurements between FM-KPFM using low frequency bias voltage and heterodyne FM-KPFM using high frequency bias voltage to demonstrate the effectiveness of HL-KPFM on the surface potential measurement. We used a silicon substrate patterned with p- and n-type impurities. We used the multi-pass scanning method in the measurements of FM-KPFM and heterodyne FM-KPFM to eliminate the effect of the tip–sample distance dependence. The measured surface potentials become lower in the order of the p-type region, n-type region and n^+-type region by both FM-KPFM and heterodyne FM-KPFM, which are in good agreement with the order of the work functions of the pn-patterned Si sample. We observed the difference in the surface potentials measured by FM-KPFM and heterodyne FM-KPFM. The difference is due to the fact that the charge transfer between the surface and bulk levels may or may not respond to AC bias voltage.

In HL-KPFM, it is expected that the bulk and surface states can be more clearly distinguished by using a low frequency bias voltage and a higher frequency bias voltage. Therefore, we believe that the HL-KPFM method can be used to characterize a variety of materials.

Funding

Grant-in-Aid for Scientific Research from Japan Society for the Promotion of Science (JSPS) from the Ministry of Education, Culture, Sports, Science and Technology (MEXT) by MEXT/JSPS KAKENHI Grant Number (16H06327, 16H06504 and 17H01061).

Conflict of interest

The authors declare that they have no conflict of interest.

References

1. Sze S M and Ng K K (2007) *Physics of Semiconductor Devices*, (New Jersey: Wiley).
2. Jeppson K O and Svensson C M (1977) Negative bias stress of MOS devices at high electric fields and degradation of MNOS devices. *J. Appl. Phys.* 48: 2004–2014.
3. Lelis A J, Habersat D, Green R, Ogunniyi A, Gurfinkel M, Suehle J, and Goldsman N (2008) Time dependence of bias-stress-induced SiC MOSFET threshold-voltage instability measurements. *IEEE Trans. Electron Devices* 55: 1835–1840.
4. Kimoto T (2015) Material science and device physics in SiC technology for high-voltage power devices. *Jpn. J. Appl. Phys.* 54: 040103.
5. Nonnenmacher M, O'Boyle M P, and Wickramasinghe H K (1991) Kelvin probe force microscopy. *Appl. Phys. Lett.* 58: 2921–2923.
6. Melitz W, Shen J, Kummel A C, and Lee S (2011) Kelvin probe force microscopy and its application. *Surf. Sci. Rep.* 66: 1–27.
7. Sadewasser S and Glatzel T (2018) *Kelvin Probe Force Microscopy from Single Charge Detection to Device Characterization. Springer Series in Surface Science*, Vol. 65, (Berlin: Springer).
8. Zhang Q Z, Li Y J, Wen H F, Adachi Y, Miyazaki M, Sugawara Y, Xu R, Cheng Z H, Brndiar J, Lev Kantorovich L, and Štich I (2018) Measurement and manipulation of the charge state of an adsorbed oxygen adatom on the rutile TiO_2(110)-1×1 surface by nc-AFM and KPFM. *J. Am. Chem. Soc.* 140: 15668–15674.
9. Adachi Y, Wen H F, Zhang Q Z, Miyazaki M, Sugawara Y, Sang H, Kantorovich L, Štich I, and Li Y J (2019) Tip-induced control of charge and molecular bonding of oxygen atoms on the rutile TiO_2 (110) surface with atomic force microscopy. *ACS Nano* 13: 6917–6924.
10. Ma Z, Kou L, Naitoh Y, Li Y J, and Sugawara Y (2013) The stray capacitance effect in Kelvin probe force microscopy using FM, AM and heterodyne AM modes. *Nanotechnology* 24: 225701.
11. Binnig G, Quate C F, and Gerber C (1986) Atomic force microscope. *Phys. Rev. Lett.* 56: 930–933.
12. Giessibl F J (1995) Atomic resolution of the silicon (111)-(7×7) surface by atomic force microscopy. *Science* 267: 68–71.
13. Sugawara Y, Ohta M, Ueyama H, and Morita S (1995) Defect motion on an InP(110) surface observed with noncontact atomic force microscopy. *Science* 270: 1646–1648.
14. Arita M, Torigoe K, Yamauchi T, Nagaoka T, Aiso T, Yamashita Y, and Motooka T (2014) Surface band-bending and Fermi-level pinning in doped Si observed by Kelvin force microscopy. *Appl. Phys. Lett.* 104: 132103.

15. Loppacher C, Zerweck U, and Eng L M (2003) Kelvin probe force microscopy of alkali chloride thin films on Au(111). *Nanotechnology* 15: S9–S13.
16. Kou L, Ma Z, Li Y J, Naitoh Y, Komiyama M, and Sugawara Y (2016) Investigation of the surface potential of TiO_2 (110) by frequency-modulation Kelvin probe force microscopy. *Nanotechnology* 27: 505704.
17. Glatzel T, Sadewasser S, Shikler R, Rosenwaks Y, and Lux-Steiner M C (2003) Kelvin probe force microscopy on III–V semiconductors: the effect of surface defects on the local work function. *Mater. Sci. Eng. B* 102: 138–142.
18. Sugawara Y, Miyazaki M, and Li Y J (2020) Surface potential measurement by heterodyne frequency modulation Kelvin probe force microscopy in MHz range. *J. Phys. Commun.* 4: 075015.
19. Sugimura H, Ishida Y, Hayashi K, Takai O, and Nakagiri N (2002) Potential shielding by the surface water layer in Kelvin probe force microscopy. *Appl. Phys. Lett.* 80: 1459–1461.
20. Nakagiri N, Sugimura H, Ishida Y, Hayashi K, and Takai O (2003) Effects of an adsorbed water layer and self-assembled organosilane monolayers on scanning probe microscopy of silicon pn structures. *Sur. Sci.* 532–535: 999–1003.
21. Barth C and Henry C R (2006) Kelvin probe force microscopy on surfaces of UHV cleaved ionic crystals. *Nanotechnology* 17: S155–S161.
22. Zou S, Yokoyama H, Sugawara Y, and Li Y J (2020) Size dependence of charge state of Pd nanoparticles on the Al_2O_3/NiAl(110) surface by Kelvin probe force microscopy. *J. Phys. Chem. C* 124: 21641–21645.
23. Shockley W and Read T (1952) Statistics of the recombinations of holes and electrons. *Phys. Rev.* 87: 835–842.
24. Kobayashi K, Yamada H, and Matsushige K (2009) Frequency noise in frequency modulation atomic force microscopy. *Rev. Sci. Instrum.* 80: 043708.